CHAPTER IV

QUANTUM DOT MOLECULES AND THEIR FORMATIONS AT DIFFERENT CAPPING-AND-REGROWTH THICKNESSES

In this chapter, we are going to discuss about the effect of capping thickness on QDM size and shape while keeping the whole processing temperature constant at 470 °C. We varied the GaAs capping thicknesses (6, 15, 25 ML) and the amounts of InAs regrowth layer (0.6, 1.2, 1.5 ML) at the growth temperature of 470 °C. When the regrowth of InAs is deposited at the appropriate thickness, QDMs are formed. At this fixed processing temperature, we are able to control dot number per molecule by choosing appropriate capping and regrowth thicknesses. The characterization of QDMs measured by AFM and PL are performed. Moreover, the explanations of the formation of nanohole, nano-propeller and QDM are also given.

4.1 Review on temperature dependence model for low dot number per QDM

According to Suraprapapich et al. [14], the effects of capping-and-regrowth temperature on the shape of ridge-hill called nano-propeller lead to the QDM with different dot numbers. The 0.3x0.3 μm^2 and 1x1 μm^2 AFM images of nano-propellers and QDMs with different capping-and-regrowth temperatures are shown in Figure 4.1. When the capping-and-regrowth temperature decreases, the dot number per molecule decreases. At lower temperature, In and Ga atoms are more difficult to move, therefore, the In-Ga intermixing rate decreases when the capping temperature decreases. In case of 430 °C, the dot number per molecule reduces to 5-6 dots. When the capping-and-regrowth temperature decreases from 470 °C to 450 °C and 430 °C, the length of nano-propeller decreases from 305 (±13) to 215 (±12) and 149 (±14) nm, respectively. The height of nano-propeller slightly decreases from 5.25 (±0.39) to 4.58 (±0.37) and 4.36 (±0.58) nm, respectively. However, there are many outside dots distributed on the surface due to the higher dislocation at lower growth temperature. The dots preferentially nucleate at steps on the surface, especially at lower substrate temperature. Since the steps are the places which have minimum energies, In atoms would be collected at steps and easily form stable 2D-islands which is the initial stage of 3D islands. The effect of the low substrate temperature provides high density with small size QDs [27]. High density QDM, which is difficult to be separated, leads to problems in quantum computing application. Consequently, the other techniques are investigated in order to improve the surface morphology and control the proper dot number per QDM.

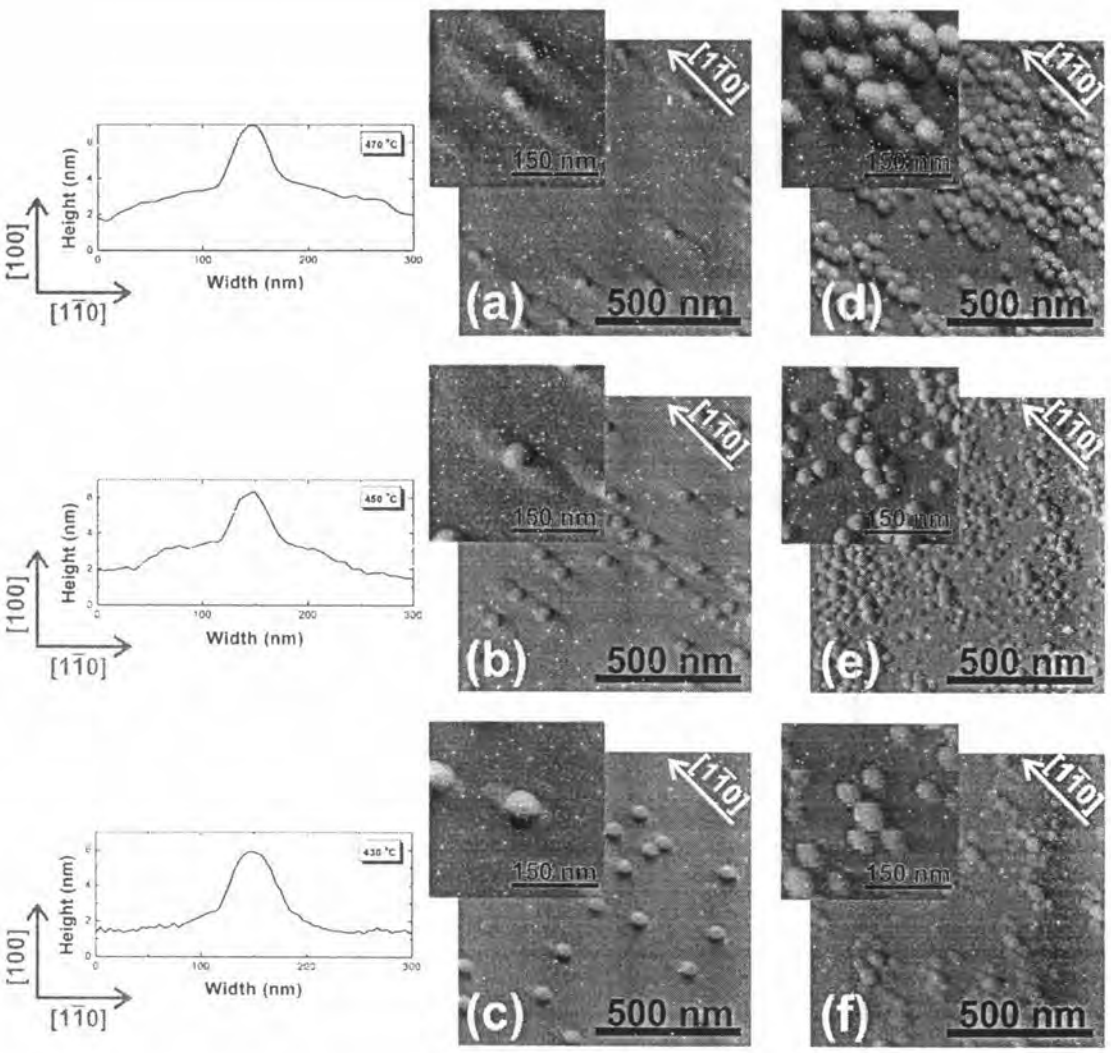

Figure 4.1: The 0.3x0.3 μm² and 1x1 μm² AFM images of nano-propellers and quantum dot molecules. The first column shows the line-scans of nano-propeller in case of 470 °C, 450 °C and 430 °C. The second column shows the AFM images of nano-propeller in case of (a) 470 °C, (b) 450 °C and (c) 430 °C. And the last column shows the AFM images of QDMs in case of (e) 470 °C, (f) 450 °C and (g) 430 °C.

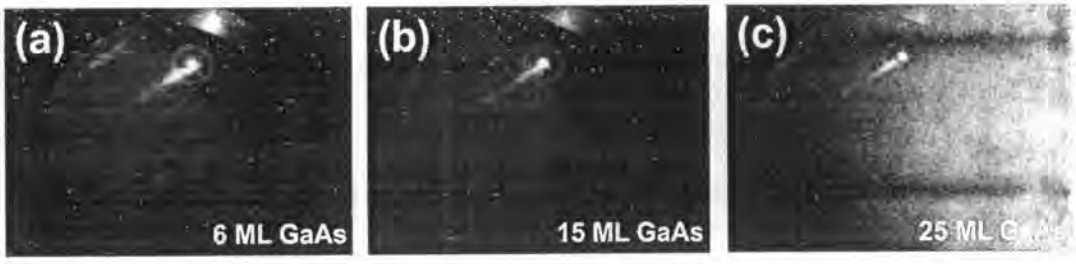

Figure 4.2: RHEED patterns of nanoholes in case of (a) 6, (b) 15 and (c) 25 ML GaAs.

4.2 Nanoholes

In our series of thin-capping-and-regrowth MBE process for QDM formation, it is found that nanohole shape, i.e. size and depth, formed after the capping stage directly impacts the shape of QDM. The two key parameters; capping-and-regrowth temperature and capping-and-regrowth thickness, are investigated. At first, 1.8 ML of InAs is deposited with 0.01 ML/s on 300-nm GaAs buffer layer at 500 °C, resulting in randomly distributed QDs across the substrate surface. The as-grown InAs QDs is then capped by a thin GaAs layer at low temperature (470 °C) which leads to nanohole templates. Low temperature capping is used to improve the homogeneity of QDs [27]. In order to obtain low growth rate QDs which have large size, the as-grown QDs are grown at high temperature. Due to the strain of large QDs are almost relaxed to the InAs lattice parameter across their tops, therefore, under GaAs overgrowth process, the central region of the QD does not undergo significant In-Ga intermixing because there is initially no GaAs growth there, and hence a higher core In fraction is retained [25]. This will be used as a well-defined template for overgrowth of QDM. We observed that the spotty pattern of dots from RHEED screen change to be broad after capping by GaAs, and then, after growth interruption around 25 sec, the diffraction pattern shows the hole shape. The snap shot of RHEED pattern of different nanoholes are shown in Figure 4.2.

The AFM images with line scans of nanoholes in case of 6 ML (17 Å), 15 ML (42 Å) and 25 ML (71 Å) GaAs are shown in Figure 4.3 (a), (b) and (c), respectively. The shape, size and depth, of nanoholes as a function of GaAs capping thickness are plotted in Figure 4.4. When we increase the thickness of GaAs capping layer from 6 to 25 ML, the base width ($\triangle X_h$) remains constant, while the base height of nanoholes ($\triangle Z_{h1}$) become shorter from 2.40 to 1.75 nm and the depth of nanoholes ($\triangle Z_{h2}$) are deeper from 0.4 to 0.6 nm. When the GaAs capping layer thickness is increased, the depth of nanoholes increases while the base length is preserved. These results coincide with the initial stages of GaAs overgrowth proposed by Joyce et al. (2001) and Songmuang (2003).

As mentioned in Joyce et al. (2001) [25], it is clear that the initial overgrowth

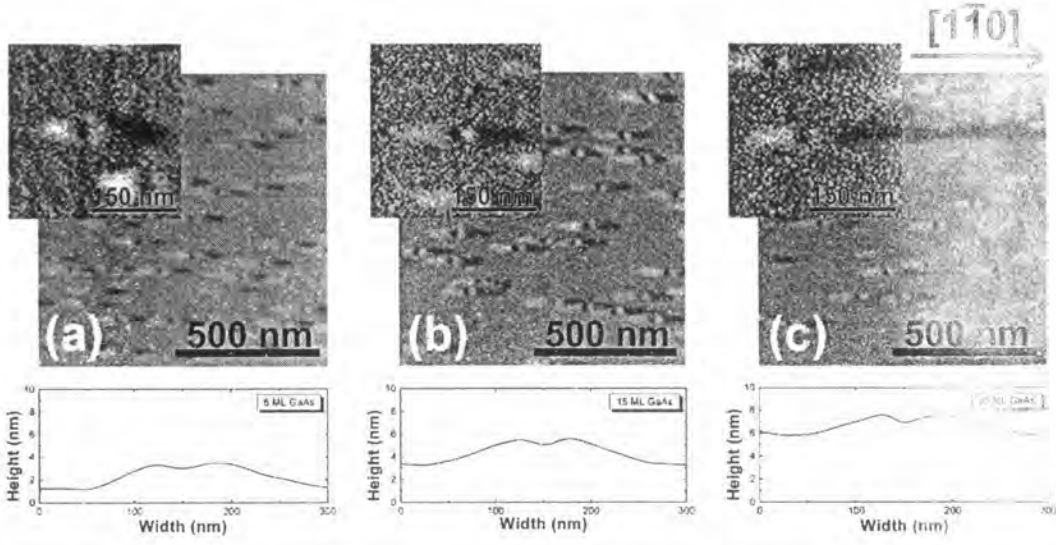

Figure 4.3: 1x1 μm^2 and 0.3x0.3 μm^2 AFM images of nanoholes with linescans in case of (a) 5 ML GaAs, (b) 15 ML GaAs and (c) 25 ML GaAs.

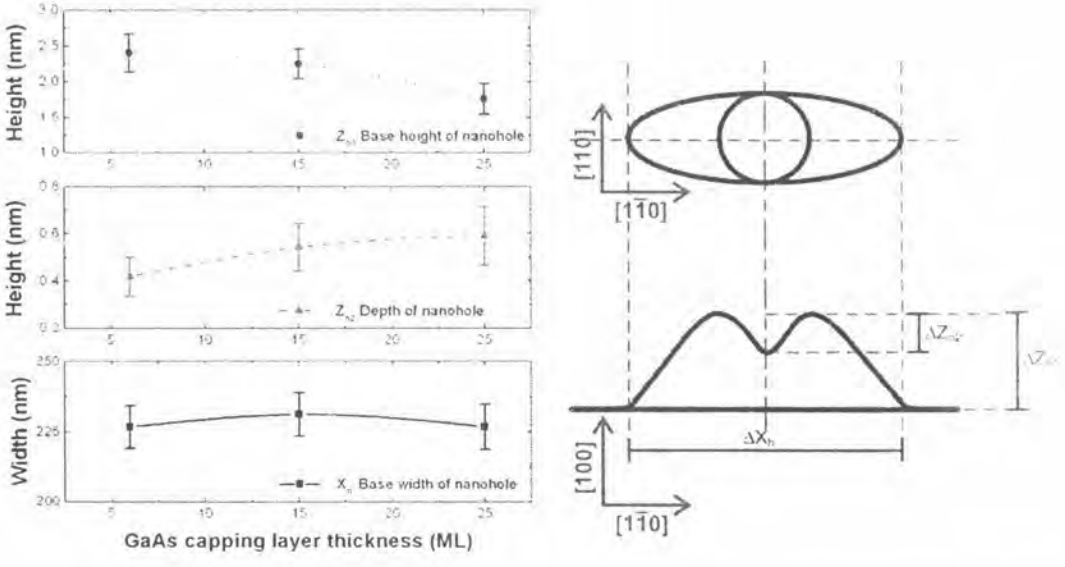

Figure 4.4: Plot of the base width (ΔX_h), base height (ΔZ_{h1}) and depth (ΔZ_{h2}) of nanoholes as a function of GaAs capping layer thickness.

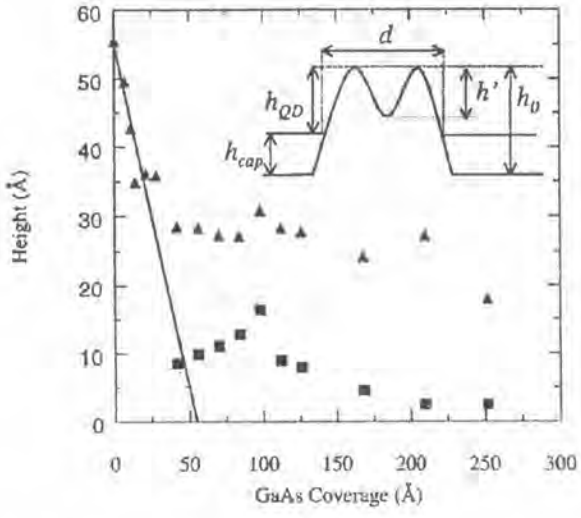

Figure 4.5: Change in mean QD or mound height [h_{QD}(▲)] and valley depth [h' (■)] as a function of GaAs capping layer thickness.. The solid line is the expected change in QD height ($h_o - h_{cap}$) assuming that the GaAs grows only around the QD. The inset is a schematic cross section of a mound with heights defined [25].

leads to major changes in surface morphology. The base area of the partially capped QDs has increased anisotropically. The QD length, along the $[1\bar{1}0]$ direction, has increased. Further deposition of GaAs leads to more dramatic changes in surface morphology. Figure 4.5 shows the change in QD height (h_{QD}) as a function of GaAs capping layer thickness (h_{cap}), as well as the depth h' of the ridge valley feature observed in the centers of the mounds. The depth of valley tends to increase when the GaAs capping layer is less than 100 Å. The solid line in Figure 4.5 indicates the expected height of the partially capped QDs if the GaAs simply grew up and around the QDs ($h_0 - h_{cap}$). At low GaAs capping thicknesses (<30 Å), the decrease in QD height is equal to $h_0 - h_{cap}$, i.e., there is no growth on top of the QDs. At greater GaAs cap thicknesses (>30 Å), however, the heights of the partially capped QDs slightly decrease despite the deposition of more than 220 Å of GaAs, indicating that growth has begun on top of the QDs.

In addition, according to Songmuang (2003) [27], the height (h) evolution of QDs as a function of the In composition and the thickness of the overlayer are summarized in Figure 4.6. The height of partially covered dots approaches the dotted line with increasing In content. An interesting result is observed if the QDs are overgrown at higher temperatures (500 °C). In this case the QDs collapse at the same rate as those overgrown at low temperature (460 °C), but the height saturates at a value close to the case of $In_{0.1}Ga_{0.9}As$ overgrowth. The inset of Figure 4.6 shows the transition from the ridge-valley to the ridge-hill structure as a function of In content in the cap layer. The inset quantities that the valley depth becomes shallower and even transforms into the

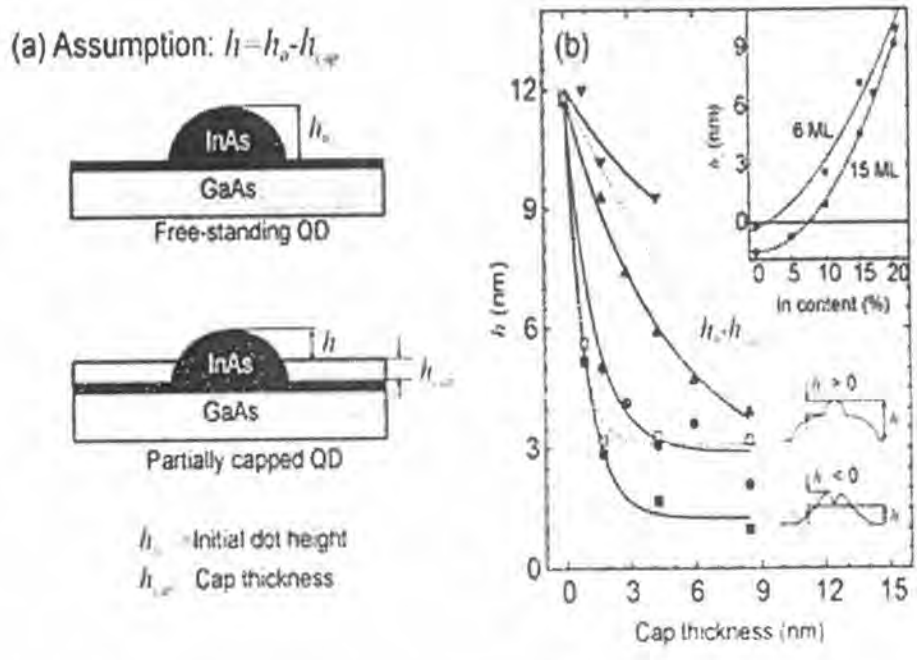

Figure 4.6: (a) The schematic showing how the QD height (h) was obtained from AFM images after GaAs overgrowth; h_0 is the initial dot height and h_{cap} is the GaAs cap thickness. (b) Height (h) of partially capped large In As QDs as a function of the cap thickness for GaAs (■), $In_{0.1}Ga_{0.9}As$ (●), $In_{0.15}Ga_{0.85}As$ (▲), $In_{0.2}Ga_{0.9}As$ (▼) with the overgrowth temperature equal to 460 °C and GaAs (❑) with the overgrowth temperature equal to 500 °C. The dotted line is the nominal height calculated from the dot height minus the cap thickness ($h_0 - h_{cap}$), assuming that the cap only surrounds the dot. The inset shows the hill height or the valley depth (h_2) as a function of In content for 6 ML and 15 ML $In_xGa_{1-x}As$ cap layer [27].

hill structure when the In content of the overlayer is increased.

The 7 % lattice mismatch between InAs and GaAs causes large strain during epitaxial growth. The strain of the system is partially released by the formation of InAs dots. However, some strains remain and affect the properties of dots and their surroundings.

After the deposition of the GaAs capping layer on the as-grown InAs QDs, the deposited Ga atoms prefer to migrate from the top of the dot, due to the lattice mismatch between GaAs and InAs at the top of QDs is higher than that between GaAs and InAs at the wetting layer. As GaAs deposition continues, the Ga adatoms become further from the InAs islands, and the growth reduction due to the strain becomes increasingly smaller due to the decaying nature of the strain fields from the islands [29].

The observed material transport away from the island surface during GaAs cap layer growth is a consequence of the surface chemical potential leading to the directional migration of adatoms on the surface. The strain field modulates the surface chemical potential for Ga adatoms as follows

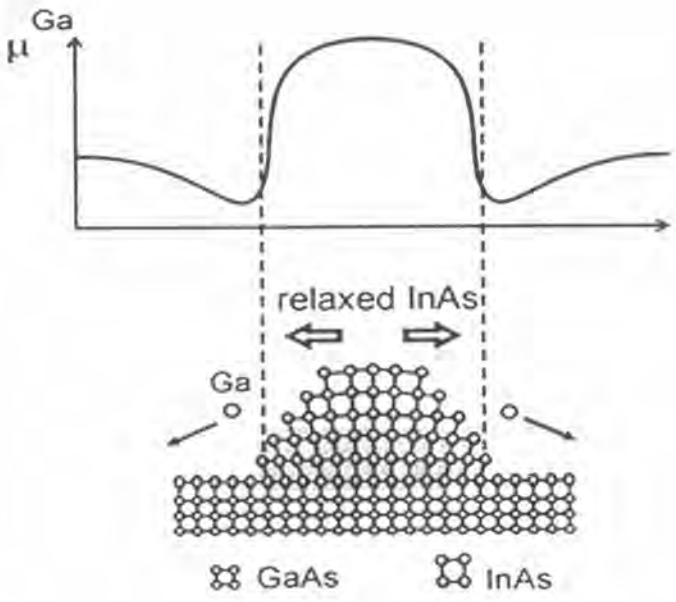

Figure 4.7: Schematic illustrations of the chemical potential of Ga atoms during the overgrowth process [27].

$$\mu^{Ga}(\mathbf{r}) = \mu_0^{Ga} + \Omega E_s(\mathbf{r}) + \gamma\Omega\kappa(\mathbf{r}) \tag{4.1}$$

where μ_0^{Ga} is the chemical potential of Ga adatoms on the reference flat surface with the lattice parameter equal to that of bulk GaAs. The second term involves the component of the surface elastic strain, $E_s(\mathbf{r})$, with Ω being the atomic volume. The third term is the surface energy contribution, where γ is the surface energy per unit area and $\kappa(\mathbf{r})$ is the surface curvature [20].

The chemical potential of Ga adatoms due to both strain and surface curvature is illustrated in Figure 4.7 [27]. The strain profile modifies the chemical potential of Ga induces net Ga migration away from the dot and reduces the growth rate of GaAs at the top of QD. This idea is experimentally confirmed by Xie et al., which their TEM image of the tilted AlGaAs marker layer and the schematic of the GaAs growth front evolution are shown in Figure 4.8.

The GaAs would cover the sides of the InAs QDs, yet some InAs QDs remains are left on the surface. The influence of the cap layer on the In atom detachment from InAs QDs can be described by position-dependent surface chemical potential [29].

The deposited GaAs covering the InAs QDs and wetting layer affects the elastic energy of the dots and the surface energy surrounding the dots. According to the SK InAs/GaAs growth mode, it is energetically favorable for InAs to evaporate from the InAs islands and to cover the free surface of GaAs, forming a second wetting layer. The

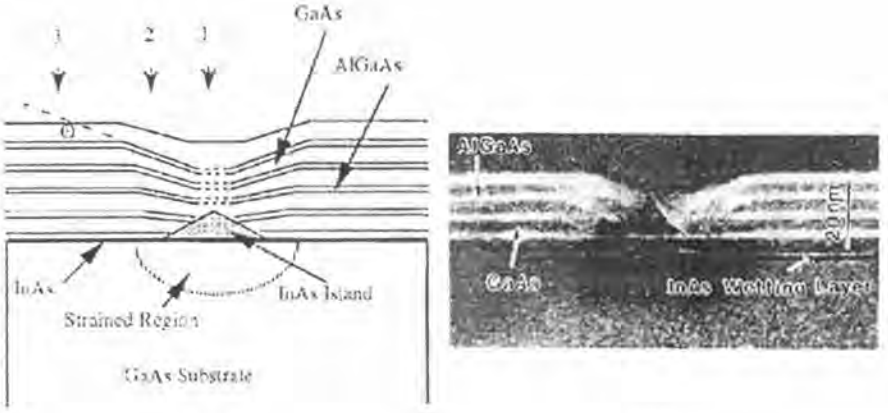

Figure 4.8: Panel (a) schematically depicts the GaAs growth front evolution and identifies. the distinct regions. Panel (b) are the TEM image showing the tilted nature of AlGaAs marker layers [29].

surface chemical potential of In atoms on partially capped InAs QDs with GaAs can be modified to

$$\mu^{In}(\mathbf{r}) = \mu_0^{In} + \Omega E_s(\mathbf{r}) + \gamma\Omega\kappa(\mathbf{r}) - \frac{\zeta\Omega\vartheta(\mathbf{r})}{a} \tag{4.2}$$

where μ_0^{In} is the chemical potential of In adatoms on an unstressed flat surface. The last term added to modify the chemical potential due to a wetting process, where ζ is the energy benefit due to the formation of a second wetting layer in the GaAs cap layer, a is the lattice parameter. and $\vartheta(\mathbf{r}) = 1$ on the GaAs surface, and $\vartheta(\mathbf{r}) = 0$ on the InAs surface. This concept was supported by the calculation of the total free energy of partially capped InAs dots with GaAs, which revealed that the reduction of the total free energy is caused by the redistribution of InAs to form second wetting layer.

In this case, following Songmuang (2003), which assumed that the local surface curvature remains unchanged when the dot is initially covered with a thin GaAs capping layer. Only the effects of the capping layer on the elastic energy and the energy benefit due to the wetting process on the chemical potential are considered, i.e., $\Omega E_s(\mathbf{r}) - \frac{\zeta\Omega\vartheta(\mathbf{r})}{a}$. For a free-standing InAs QD, $\vartheta(\mathbf{r}) = 0$ at every position. The elastic relaxation of the QD causes high strain energy at the QD edge [30]. The schematic illustration of estimated chemical potential of In adatoms both capped and uncapped QDs are shown in Figure 4.9

After capped, the dot base becomes more compressed by the surrounding GaAs and consequently increased the surface elastic energy. The increase of the surface energy due to the surrounding GaAs layer also induces the detached In atoms to the thin GaAs capping layer surface. Therefore, the change of the elastic energy and the surface energy during the overgrowth process cause the dissolution and the collapse of

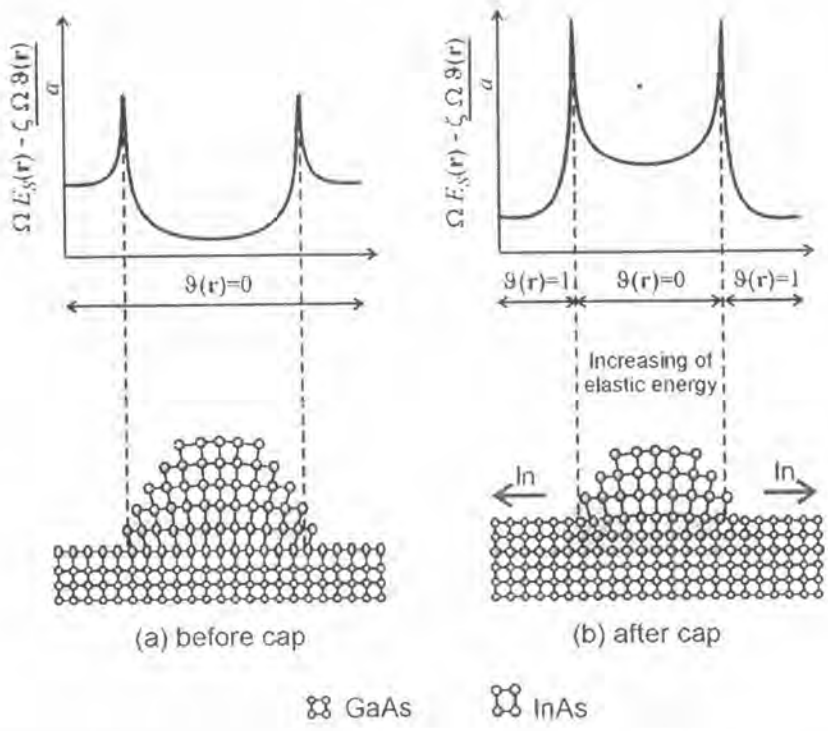

Figure 4.9: Schematic illustrations of the term $\Omega E_s(\mathbf{r}) - \frac{\zeta \Omega \vartheta(\mathbf{r})}{a}$ for (a) free-standing (b) partially capped InAs QDs with thin GaAs [27].

the InAs QDs resulting in the ridge-valley structure formation [27]. Moreover, when the GaAs capping layer is thicker, more In atoms are pulled out from the dots, leading to the increase nanoholes depth (ΔZ_{h2}).

To confirm the mechanism of nanoholes formation, the power dependence of QDs and 6 ML GaAs nanoholes are performed, as shown in Figure 4.10. The peak emissions of QDs and nanoholes appear at 1.08 eV and 1.20 eV, respectively. As described in Figure 3.11, the ground state PL peak emission contains information about the size of QD. Increasing of QD size results in lower quantized energy levels, which leads to a lower PL peak position. Therefore, it can be interpreted that, after capping, QD is collapsed due to the In atom diffused out from dot resulting in the reduction of QD size. PL of 6 ML GaAs nanoholes exhibits a relatively strong wetting layer PL signal. This is probably due to the low density of InAs QDs and hence relatively lower QD emission [31].

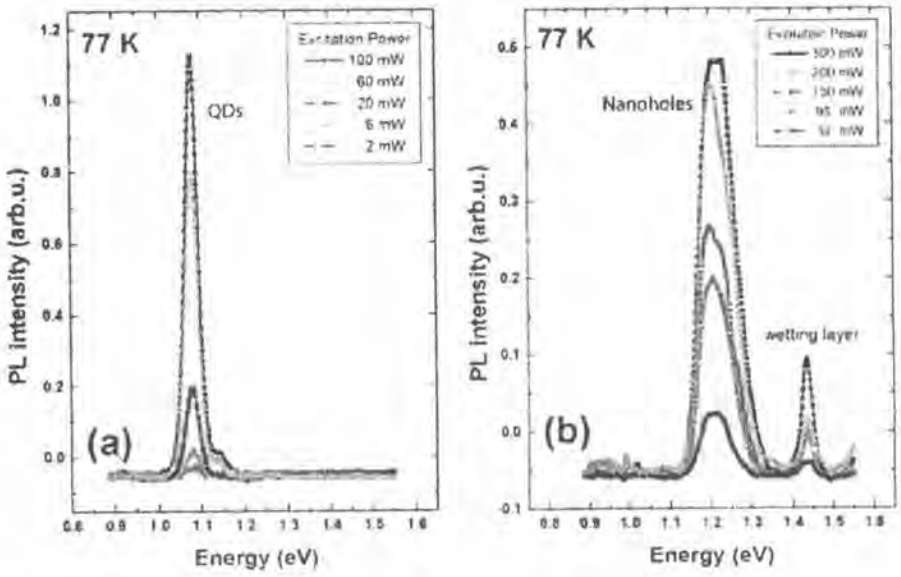

Figure 4.10: Power dependent PL spectra of QDs (a) and 6 ML GaAs nanoholes (b) at 77 K.

4.3 Nano-propellers

Subsequent regrowth of 0.6 ML InAs on nanoholes results in nano-propeller QDs with alignment along the $[1\bar{1}0]$ crystallographic directions. The In adatoms would attach to the center of the nanohole due to the highest In content of remained QD after capping process. The AFM images with linescans of nano-propellers in case of 6, 15, 25 ML GaAs are shown in Figure 4.11 (a), (b) and (c), respectively, where the shape, height and length of nano-propellers as a function of GaAs capping thickness are plotted in Figures 4.12. During this early stage, when the QD of nano-propellers are not saturated, the deeper nanoholes give smaller dots due to the smaller remained InAs islands at the center of nanoholes. As shown in Figure 4.11, $\triangle Z_p$ decreases from 6 nm to 4 nm. The variation of capping thickness (6 to 25ML) defines also the length of nano-propeller blades ($\triangle X_p$) from 300 to 200 nm. After the strain at the center of nanohole are partially relaxed by In adatoms, the In atoms migrate away to the base side of nanoholes. We proposed that, at the thinner capping layer, the In content at the base side is higher due to the lower Ga atoms at the surface resulting in In atoms accumulate because of the lower mismatch between InAs and $In_xGa_{1-x}As$. The more In atoms are accumulated, the larger blade are formed.

Therefore, we used the model of free standing QD capped by $In_xGa_{1-x}As$ to explain the tendency of In adatoms migration after this early regrowth stage [27]. When the overgrowth material was changed from GaAs to $In_xGa_{1-x}As$, the In content in the $In_xGa_{1-x}As$ cap layer affects both the elastic energy contribution and the energy benefit from the wetting process in eq. 4.2. By increasing the In content on the $In_xGa_{1-x}As$ cap layer, the lattice mismatch between the cap and the QD decreases,

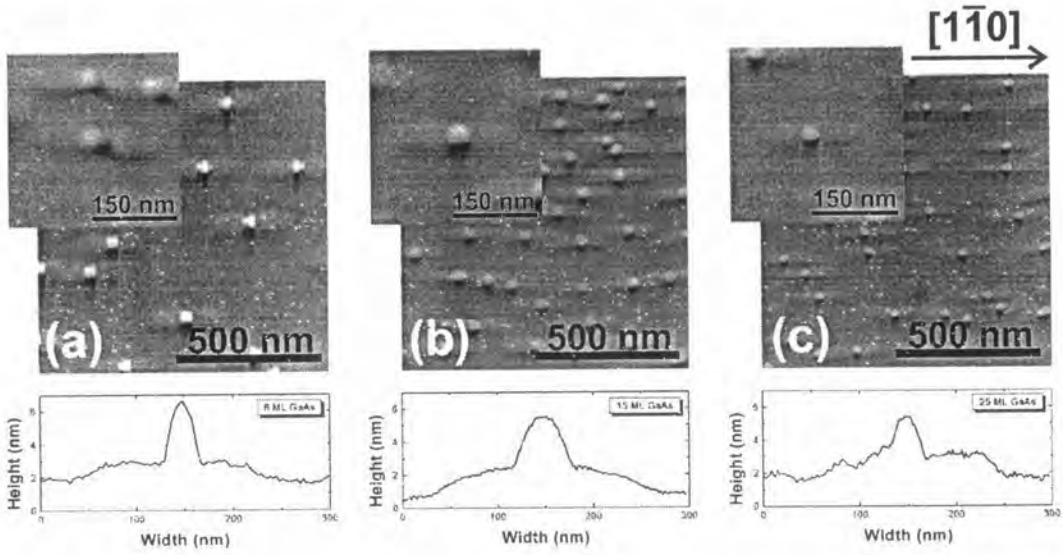

Figure 4.11: 1x1 μm^2 and 0.3x0.3 μm^2 AFM images of nano-propellers with linescans in case of (a) 6 ML GaAs, (b) 15 ML GaAs and (c) 25 ML GaAs.

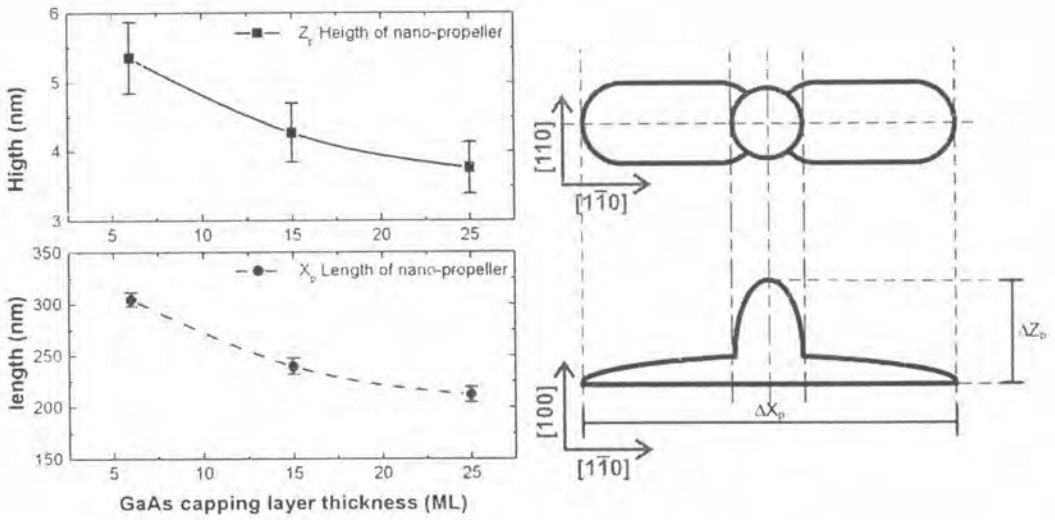

Figure 4.12: Plot of the height (ΔZ_p) and length ΔX_p of nano-propellers as a function of GaAs capping layer thickness.

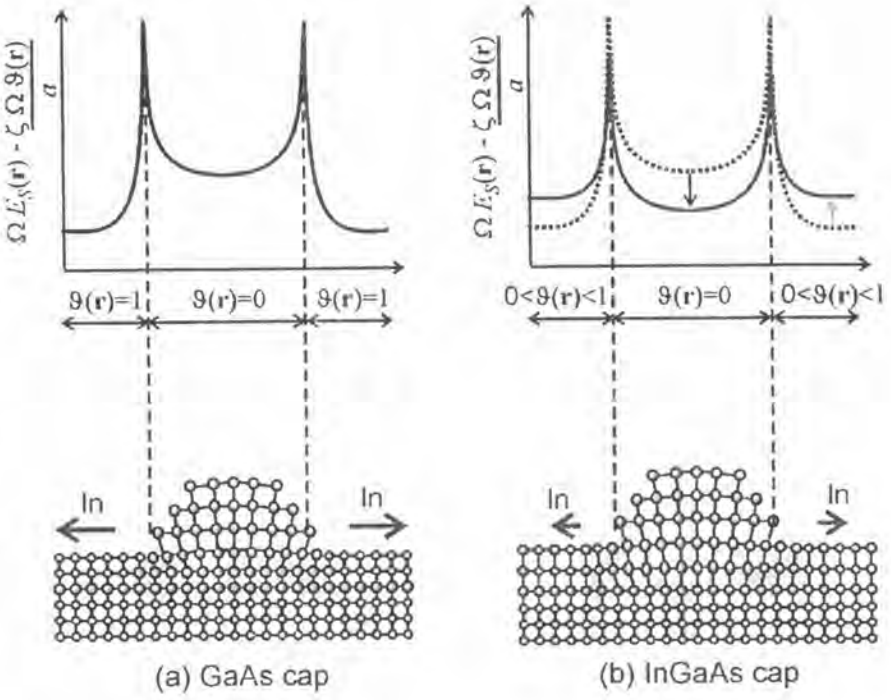

Figure 4.13: Schematic illustrations of the term $\Omega E_s(\mathbf{r}) - \frac{\zeta\Omega\vartheta(\mathbf{r})}{a}$ for partially capped InAs QDs with (a) thin GaAs (b) thin InGaAs [27].

resulting in an elastic energy reduction. Moreover, the tendency of In atoms to cover the free cap surface decreases with high In content (it might be estimated the effect of In content by interpolating $\vartheta(\mathbf{r})$ value between 0 and 1, depending on the In content). The $In_xGa_{1-x}As$ cap layer therefore decreases the In atom detachment rate and the migration of In atoms away from the QD to the cap surface. The schematic in Figure 4.13 illustrates the effect of InGaAs cap layer to $\Omega E_s(\mathbf{r}) - \frac{\zeta\Omega\vartheta(\mathbf{r})}{a}$. The shorter blades yield less dot number per QDM when the regrowth process is continued to create more satellite dots at InAs thickness of 1.2 and 1.5 ML, as shown in next section.

4.4 Quantum dot molecules (QDMs)

When the amount of InAs regrowth layer increases from 0.6 to 1.2 and 1.5 ML, QDMs with different shapes are created. The AFM images of QDMs created after 1.2 ML and 1.5 ML InAs deposited on nanoholes with different GaAs capping thicknesses are shown in Figure 4.14. The center dots are formed by filling up nanoholes at the beginning phase until the strain relaxation at center becomes minimized. Later on, the rest of InAs regrowth material starts to form satellite dots along the blade of nano-propeller where remaining strain fields are still distributed at the perimeter of nano-propeller blades. The schematic of QDM formation are illustrated in Figure 4.15 We observed that if the blade size of nano-propeller is large and long, the number of satellite

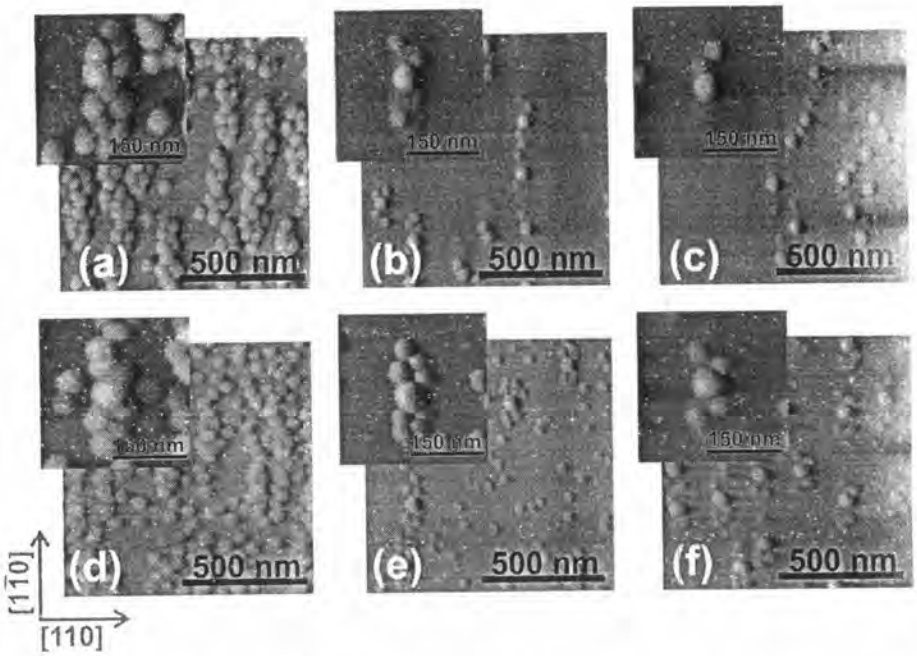

Figure 4.14: 1x1 μm^2 and 0.3x0.3 μm^2 AFM images of QDMs created after deposited different InAs regrowth thicknesses on nanoholes at different GaAs capping thicknesses, (a) 6 ML GaAs capping layer and 1.2 ML InAs regrowth layer, (b) 15 ML GaAs capping layer and 1.2 ML InAs regrowth layer, (c) 25 ML GaAs capping layer and 1.2 ML InAs regrowth layer, (d) 6 ML GaAs capping layer and 1.5 ML InAs regrowth layer, (e) 15 ML GaAs capping layer and 1.5 ML InAs regrowth layer, (f) 25 ML GaAs capping layer and 1.5 ML InAs regrowth layer, respectively.

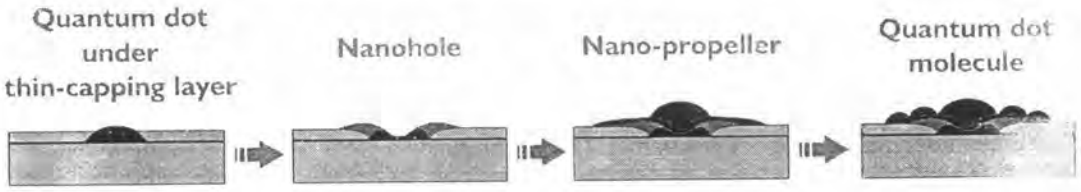

Figure 4.15: Schematic of growth step of QDM.

dots is likely to be high.

Figure 4.14 (a) shows the saturated formation having 10-12 dots per QDM at 6 ML GaAs capping thickness and 1.2 ML InAs regrowth thickness. If the regrowth thickness is increased more than a critical value, high density QDM is obtained, as shown in Figure 4.14 (d) where the regrowth thickness is set up at 1.5 ML. When the regrowth thickness is 1.2 ML and the capping thickness is between 15 and 25 ML, QDM formation is not saturated, therefore, small dot number of 3-4 dots per QDM is observed, as shown in Figures 4.14 (b) and (c). Until the regrowth thickness is farther increased to 1.5 ML, the dot numbers increase to 8-9 and 5-6 dots per QDM at capping layers of 15 and 25 ML, as shown in Figures 4.14 (e) and (f), respectively. It is concluded that the thicker capping layer, the more critical regrowth thickness used to form the saturated QDM. However, when the amount of InAs is greater than a critical

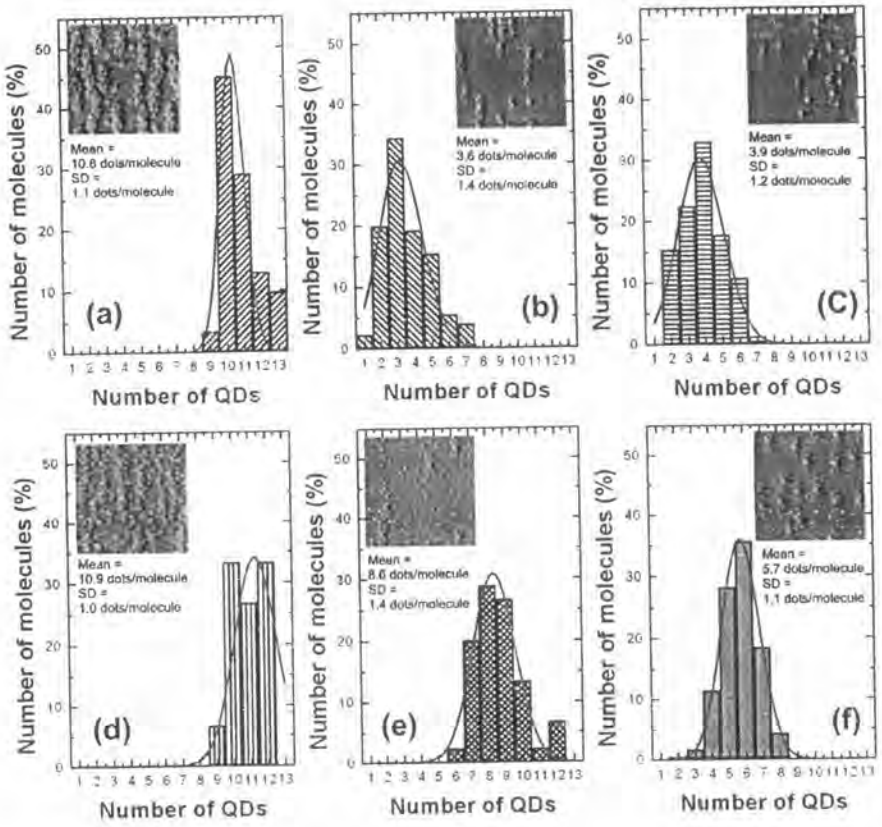

Figure 4.16: The statistical results of dot number per QDM in selected samples at different capping thicknesses and different regrowth thicknesses: (a) 6 ML GaAs capping layer and 1.2 ML InAs regrowth layer, (b) 15 ML GaAs capping layer and 1.2 ML InAs regrowth layer, (c) 25 ML GaAs capping layer and 1.2 ML InAs regrowth layer, (d) 6 ML GaAs capping layer and 1.5 ML InAs regrowth layer, (e) 15 ML GaAs capping layer and 1.5 ML InAs regrowth layer, (f) 25 ML GaAs capping layer and 1.5 ML InAs regrowth layer, respectively.

regrowth thickness, the high dot density is obtained resulting in less uniform QDM.

The height distribution is investigated. The height distribution of center dots and satellite dots of samples in Figures 4.14 (a)-(c) are illustrated in Figures 4.17 (a)-(c). When the GaAs capping thickness increases, the center dot height increases, as the satellite dot decreases. Therefore, the hight difference between center dot and satellite dot tend to increase when the GaAs capping thickness become thicker.

The statistical results of dot number per QDM in selected samples at different capping thicknesses and different regrowth thicknesses are shown in Figure 4.16. The percentages of QDMs in accordance with QCA (5 dots per molecule) in case of samples in Figure 4.16 (b), (c) and (f) are 15, 18 and 28 %, respectively. It can be concluded that 25 ML GaAs capping layer thickness is more appropriate than 15 ML. However, there is a lot of height difference between center dot and satellite dot in case of 25 ML GaAs and 1.5 ML InAs (sample in Figure 4.16 (f)). The height distribution in case of 25 ML GaAs and 1.5 ML InAs is illustrated in Figure 4.18. The center dot and satellite dot height

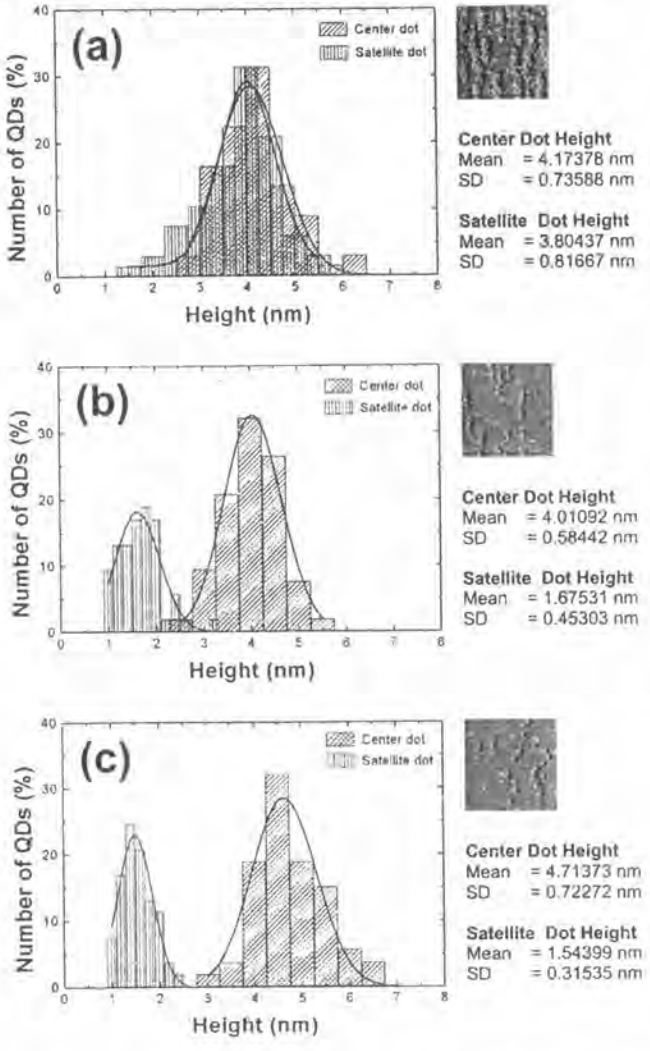

Figure 4.17: Histograms of height distribution of center dots and satellite dots with 1x1 μm^2 AFM images at 1.2 ML InAs regrowth layer and different GaAs capping layer thicknesses: (a) 6 ML, (b) 15 ML and (c) 25 ML GaAs.

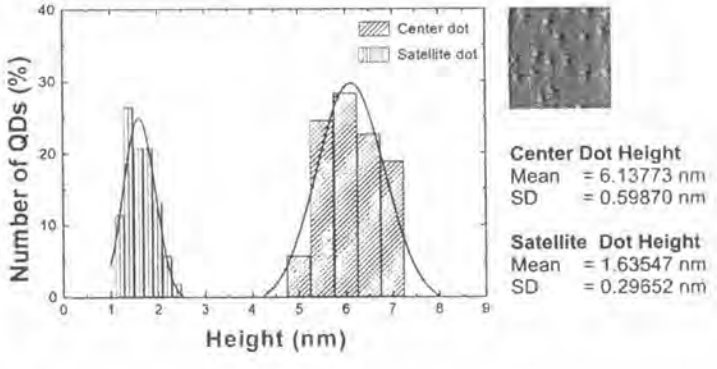

Figure 4.18: Histogram of height distribution of center dots and satellite dots with 1x1 μm^2 AFM images at 1.5 ML InAs regrowth layer and 25 ML GaAs capping layer thickness

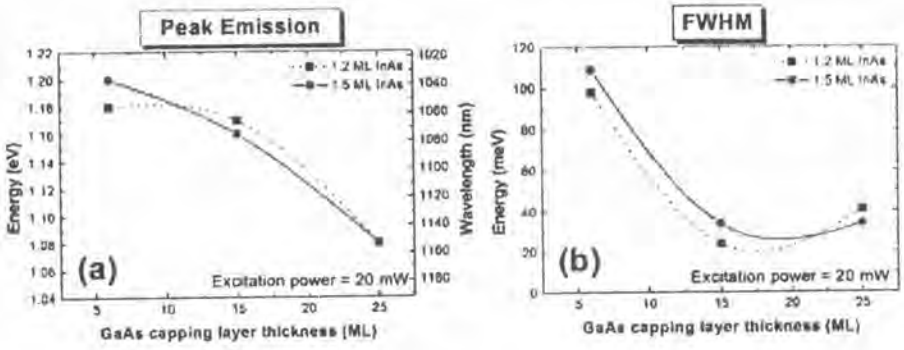

Figure 4.19: PL results, (a) peak emissions and (b) FWHM, of samples grown with the InAs regrowth layer thickness of 1.2 ML and 1.5 ML at 77 K.

become bigger compared to QDM in case of 25 ML GaAs and 1.2 ML InAs (Figure 4.17 (c)). To create an optimum shape of nanoholes upon which subsequent QDs, both center and satellite dots, would be grown to the same size with good uniformity which is the ideal case for practical QDMs. The modified QDM by using thermal energy is investigated in Appendix.

In order to confirmed the homogeneity of QDMs in different cases, the PL measurements were performed. All QDM samples with different thicknesses of GaAs capping layers (6, 15, 25 ML) at regrowth thicknesses of 1.2 ML (sample A-C) and 1.5 ML (sample D-F) are tested for their photoluminescence spectra at 77 K, as illustrated in Figure 4.19. When all samples are excited by an Argon laser excitation power of 20 mW, the ground-state peak emissions of samples A, B and C appear at 1.18, 1.17 and 1.08 eV with the FWHM of 98, 24 and 41 meV respectively, as shown in Figure 4.19 (a). The redshift of PL peak from the sample C with GaAs capping thickness of 25 ML indicates that the dot size is larger than those of another two samples A and B with 6 and 15 ML capping thicknesses, respectively. Sample A has broad spectrum due to less dot uniformity which is confirmed by its AFM image. Sample B has narrower spectrum than sample C because of its better dot uniformity.

Figure 4.19 shows the PL results from sample D-F with regrowth thickness of 1.5 ML. Their ground-state peak emissions are at 1.20, 1.16 and 1.08 eV, respectively. Clear redshift, which indicates the increase in dot size, is confirmed in this series of samples due to the saturated QDM formation. The FWHM of PL spectra of samples D-F are 109, 34 and 34 meV, respectively. Sample D, with regrowth thickness more than a critical thickness, has broad PL spectrum due to less dot uniformity.

In addition, in case of different GaAs capping layer thicknesses by keeping the regrowth layer constant at 1.2 ML InAs, we observed that the decreasing of ground state peak emission energy (Figure 4.19 (a)) exhibits in accordance with that of height distribution of center dot (Figure 4.17).

The excitation power dependence of PL spectra of all samples is also conducted.

The PL results of QDMs with different capping thicknesses and different regrowth thickness are shown in Figure 4.20. It can be obviously seen that, the ground state peak emission of center dot at low excitation power in each case would appear first. And then, if the excitation energy increase, the first excited state of center dot and ground state and the higher excited states exhibit. This is properly due to the fact that, at first, the satellite dot with bigger energy gap let photons pass and the center dot with lower energy gap absorb the photons. After the ground state of center dot fulled, the rest power excitation are absorbed by the dots with higher energy gaps.

However, the observed results are in contrast with spectra observed from as-grown quantum dots. These results are explained by state filling in the presence of extended electron states formed due to lateral electronic coupling of the QDs within the QDMs. The coupling among QDs leads to a splitting of the quantized carrier energy levels of single dots and formation of three-dimensional minibands. By changing the size of QDts, interdot distances, barrier height, and regimentation, one can control the electronic band structure of this artificial QD crystal [32].

According to Lippen (2006), the asymmetric broadening together with the shift of the PL peak towards higher energies are first indications for the formation of extended states in the QDMs due to tunnel coupling. Tunnel coupling of the QD ground states creates extended states with a distinct energy separation determined by the coupling strength. State filling with increase of the excitation power density then accounts for the asymmetric broadening of the PL spectrum with unchanged low energy side [33].

The appearance of excited state emission with increasing excitation power density from the QDMs is likely blurred by the asymmetric broadening and high-energy shift of the PL peak. Hence, the behaviour of the QDMs is in marked contrast to that of ensembles of isolated QDs. There, with increasing excitation power density, the PL line shape and peak energy of the QD ground state emission remain unchanged, as can be seen for the reference sample with as-grown InAs QDs, or even slightly shifts to lower energy due to Coulomb interaction and emission peaks from excited states appear at higher energies due to state filling [33].

Our PL results from some case of different QDMs also exhibit the shift of the PL peaks toward higher energies. We believe that the coupling between center dot and satellite dots lead to the extending in band structures. The plot between excitation power and PL peak position, and excitation power and integrated PL intensity are illustrated in Figure 4.21 (a) and (b), respectively. The PL peak positions in most cases tend to increase to the higher energy states when the excitation power increases. In case of sample B, however, the peak shifted to the lower energy. We proposed that this shift is originated from the larger separation between center dot and satellite dots as shown in Figure 4.14. However, the resolution of our PL set-up can not clearly present the coupling at 77 K. Therefore the experiments at lower temperature (7-10 K) should to be conducted.

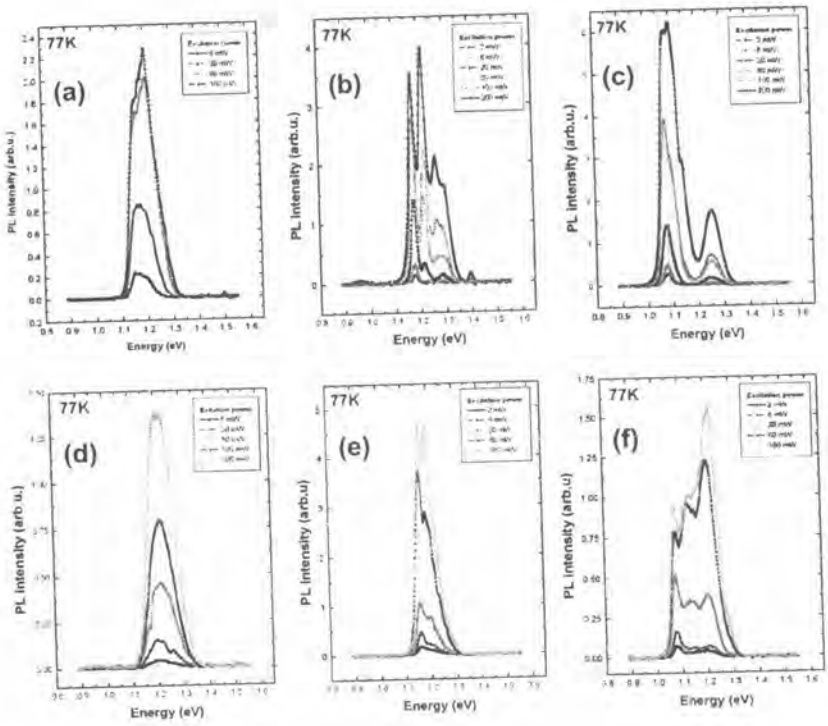

Figure 4.20: Power dependent PL spectra of different QDMs at 77 K: (a) 6 ML GaAs capping layer and 1.2 ML InAs regrowth layer, (b) 15 ML GaAs capping layer and 1.2 ML InAs regrowth layer, (c) 25 ML GaAs capping layer and 1.2 ML InAs regrowth layer, (d) 6 ML GaAs capping layer and 1.5 ML InAs regrowth layer, (e) 15 ML GaAs capping layer and 1.5 ML InAs regrowth layer, (f) 25 ML GaAs capping layer and 1.5 ML InAs regrowth layer, respectively.

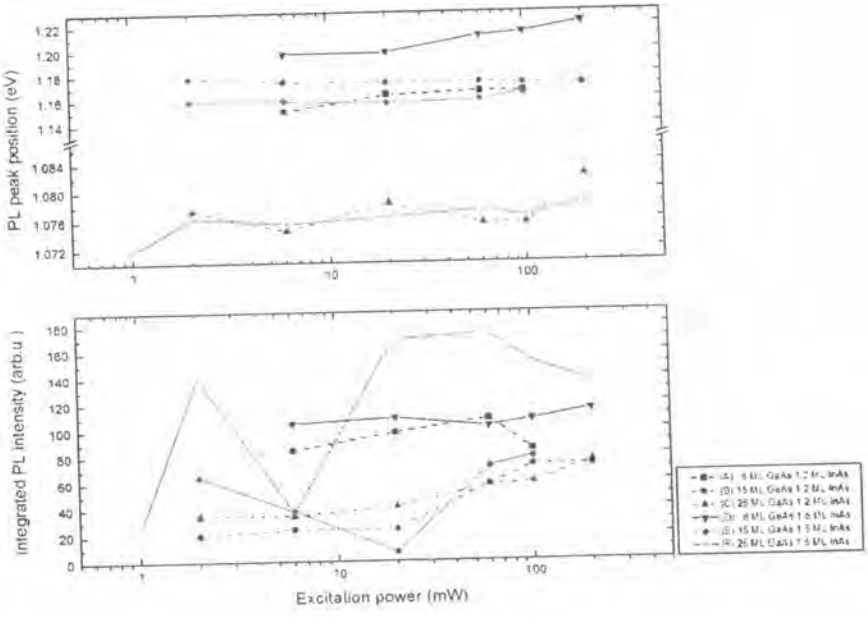

Figure 4.21: (a) The plot between excitation power and peak emission position. (b) The plot between excitation power and integrated PL intensity.